Eur. Phys. J. B **11**, 91–100 (1999)

THE EUROPEAN PHYSICAL JOURNAL B

EDP Sciences

Lattice-Boltzmann study of spontaneous emulsification

O. Theissen and G. Gompper[a]

Max-Planck-Institut für Kolloid- und Grenzflächenforschung, Am Mühlenberg, Haus 2, 14476 Golm, Germany

Received 5 January 1999

Abstract. We study the dynamics of spontaneous emulsification of an initially planar oil-water interface when surfactants are added. The thermodynamic properties of the ternary oil-water-surfactant system are modeled by a Ginzburg-Landau-type free energy. The lattice Boltzmann method is used to solve the dynamic equations. The dynamics is found to be governed by a complicated interplay of convection and diffusion as the two relevant transport mechanisms. As long as the interface is almost flat, we find the interfacial area to grow first exponentially and then linearly in time. Later finger-like structures form which grow with a constant velocity. The tip velocity is found to increase roughly linearly with the mobility of the amphiphile, and to decrease as $\nu^{-1/2}$ with the solvent viscosity ν.

PACS. 82.70.Kj Emulsions and suspensions – 47.20.Dr Surface-tension-driven instability – 83.10.Lk Multiphase flows

1 Introduction

Two immiscible fluids, *e.g.* oil and water, can be mixed on mesoscopic length scales by adding surfactants. The resulting arrangements of oil and water domains can be hexagonal, lamellar or disordered (microemulsion) [1,2]. The process of transformation from a macroscopically phase-separated state to a mesoscopically mixed state is called *spontaneous emulsification*. The term spontaneous refers to the fact that no stirring or shaking is required to start the emulsification process. In this respect, emulsification can be viewed as an instability.

Despite its relevance for industrial processes and everyday life, the understanding of spontaneous emulsification is rather poor from a physical point of view. All experimental studies [3–10] done so far remain on an empirical level. Theoretically, the process of spontaneous emulsification has been addressed by Sorensen [11] and by Granek, Ball and Cates [12]. Only the latter study includes the bending rigidity, which is believed to be essential in surfactant systems.

The experimental and theoretical studies mentioned above give an intuitive picture about the physics of spontaneous emulsification. Initially, there are two coexisting regions of oil and water separated by an almost planar interface. By adding surfactants, the surface tension of the oil-water interface is lowered approximately proportional to the concentration of the surfactant at the interface. When the surface tension finally becomes slightly negative, the interface becomes unstable. This gives rise to a *hydrodynamic instability*, controlled by the viscosity ν, the surface tension σ and bending rigidity κ of the interface. Standard hydrodynamic stability analysis [13,14] predicts that the deviation $h(\mathbf{r};t)$ of the local interface position from the initial reference state grows exponentially, $h(\mathbf{k};t) \propto \mathrm{e}^{\lambda(k)t}$, with

$$\lambda(k) = -\frac{1}{4\nu}(\sigma k + \kappa k^3) \tag{1}$$

where k is the wave number of the excited mode. This behavior cannot last forever. First, because equation (1) is based on a linear stability analysis, and second, because the surface tension becomes a dynamic quantity itself. Since the interfacial area is growing due to the instability, the concentration of surfactant at the interface is lowered, the surface tension increases again and thus the driving force decreases. As there is usually a finite concentration of surfactant dissolved in the bulk oil and water phases, *diffusion* acts as a transport mechanism to resupply surfactant to the interface. One may therefore expect a diffusion limited growth of the interface; indeed, this is the behavior found by Granek, Ball and Cates [12].

In addition, another mechanism may become relevant — *convection*. As the unstable interface propagates into the bulk oil or water regions the surfactants which are dissolved in the bulk phases may either be "picked up" by the interface or be convected into the vicinity of the interface. We will report evidence for convection to be relevant for spontaneous emulsification.

The situation for spontaneous emulsification has to be contrasted with other dynamic instabilities like dendritic growth, where convection can be neglected due to the hydrodynamic boundary layer around solid clusters or dendrites [15].

The purpose of this paper is to elucidate the dynamics of spontaneous emulsification in its initial and late

[a] e-mail: gompper@mpikg-golm.mpg.de

stages. Thereby we take both the thermodynamic behavior and the complete set of hydrodynamic transport equations into account. This is done by using the lattice Boltzmann method [16–23] for the dynamics combined with a Ginzburg-Landau model [24–26] for the thermodynamics. We restrict ourselves to two dimensions in order to minimize the computational effort.

2 The model

As mentioned above, the theoretical modeling has to meet two challenges. First, one has to get the thermodynamics of the ternary system oil, water and surfactant right. In particular, a surfactant concentration-dependent surface tension of the oil-water interface and its bending rigidity have to be contained in the model. Second, one has to take both convection and diffusion as transport mechanisms into account.

The thermodynamic part can successfully be described by a Ginzburg-Landau free-energy functional

$$\mathcal{F}[\rho,\phi,\psi] = \omega \int \mathrm{d}^d x \Big\{ T\rho\ln\rho + g_\phi(\nabla\phi)^2 + (\phi^2-\phi_b^2)^2 + g_\psi(\nabla\psi)^2 + s\psi^2 + \gamma_1\psi\phi^2 + \gamma_2 l^2\psi(\nabla\phi)^2 + \gamma_3 l^4\psi(\nabla^2\phi)^2 \Big\}, \quad (2)$$

which depends on the mass density $\rho > 0$ of the fluid, the difference ϕ of oil and water densities, and the surfactant density $\psi > 0$ [24–26]. The mass density ρ gives rise to a positive background pressure and does not affect the phase behavior. It is therefore usually not included in Ginzburg-Landau theories, but is required in the lattice Boltzmann approach [23,22] described in Section 3. We explicitly take into account the length l of the surfactants in the free energy. The l-dependence of the coefficients in the free-energy functional has been derived in reference [27] from a mapping of a "microscopic" spin model, in which the surfactants are taken to be dipoles of length l, onto a Ginzburg-Landau theory with a *single* order parameter. Here we adopt this result to our *three* order parameter model by identifying the appropriate leading powers of l.

The parameters are chosen such that the equilibrium state is the lamellar phase not far from oil-water coexistence for an average surfactant concentration of $\psi = 0.05$: $g_\phi = 0.5$, $g_\psi = 2.0$, $\phi_b = 0.5$, $s = 2.0$, $\gamma_1 = 2.0$, $\gamma_2 = -4.0$, $\gamma_3 = 1.0$ and $l = 1.2$. The background pressure ρT is controlled by $T = 0.5$, and $\omega = 0.01$ sets the scale of the free energy.

The dynamics is described by the incompressible Navier-Stokes equation with kinematic viscosity ν and pressure p,

$$\nabla\cdot\mathbf{v} = 0, \quad (3)$$

$$\partial_t\mathbf{v} + \mathbf{v}\cdot\nabla\mathbf{v} = -\frac{1}{\rho}\nabla p + \nu\nabla^2\mathbf{v}, \quad (4)$$

and for each of the fields ϕ and ψ by a *convection-diffusion* equation,

$$\partial_t\phi + \mathbf{v}\cdot\nabla\phi = \Gamma_\phi\nabla^2\frac{\delta\mathcal{F}}{\delta\phi}, \quad (5)$$

$$\partial_t\psi + \mathbf{v}\cdot\nabla\psi = \Gamma_\psi\nabla^2\frac{\delta\mathcal{F}}{\delta\psi}, \quad (6)$$

where Γ_ϕ and Γ_ψ are the mobilities. Note that it is crucial to keep the coupling of the convective flow to the diffusion in equations (5, 6).

A suitable approach for solving such equations numerically while incorporating the correct thermodynamic behavior was introduced by Orlandini, Swift, and Yeomans [28,21] using a lattice Boltzmann model. This method has successfully been applied to amphiphilic systems in references [29–31]. In Section 3 we give a brief description of the lattice Boltzmann approach.

The main difficulty in combining the thermodynamics given by equation (2) and the lattice Boltzmann approach is to find the equations of state. For an isothermal, ternary fluid there are three equations of state. Two equations for the chemical potentials,

$$\mu_\phi = \frac{\delta\mathcal{F}}{\delta\phi} \quad \text{and} \quad \mu_\psi = \frac{\delta\mathcal{F}}{\delta\psi}, \quad (7)$$

which are straightforward to calculate, and one equation for the pressure, which is not trivial to derive. As interfaces in the fluid can exert non-isotropic forces, the pressure is not a scalar, but a tensor $P_{\alpha\beta}$. Thermodynamics provides only an expression for the scalar part p_0 of $P_{\alpha\beta}$, which is given by the usual thermodynamic relation

$$p_0 = -\left(\frac{\partial F}{\partial V}\right)_T = \rho\frac{\delta\mathcal{F}}{\delta\rho} + \phi\frac{\delta\mathcal{F}}{\delta\phi} + \psi\frac{\delta\mathcal{F}}{\delta\psi} - f(\rho,\phi,\psi). \quad (8)$$

Here, $f(\rho,\phi,\psi)$ is the free energy density, *i.e.* the integrand in equation (2). Unfortunately there is no formula known to calculate the complete pressure tensor $P_{\alpha\beta}$. It is the requirement of *mechanical equilibrium*,

$$\partial_\beta P_{\alpha\beta} = \rho\partial_\alpha\frac{\delta\mathcal{F}}{\delta\rho} + \phi\partial_\alpha\frac{\delta\mathcal{F}}{\delta\phi} + \psi\partial_\alpha\frac{\delta\mathcal{F}}{\delta\psi}, \quad (9)$$

which provides at least a necessary condition for $P_{\alpha\beta}$ [32]. Our procedure to determine $P_{\alpha\beta}$ is as follows. The pressure tensor is written as

$$P_{\alpha\beta} = p_0\delta_{\alpha\beta} + \tilde{P}_{\alpha\beta} \quad (10)$$

where p_0 is determined by equation (8), and the anisotropic part $\tilde{P}_{\alpha\beta}$ is chosen such as to fulfill equation (9) and to vanish for spatially homogeneous systems. However, note that equation (9) does *not* determine $\tilde{P}_{\alpha\beta}$ uniquely; an arbitrary tensor $\Lambda_{\alpha\beta}$ can be added as long as its divergence, $\partial_\beta\Lambda_{\alpha\beta}$, vanishes. In practice, we proceed by making an ansatz for $\tilde{P}_{\alpha\beta}$, which includes all powers of the fields and their derivatives which are allowed for dimensional reasons. This ansatz is inserted into equation (9)

to determine the unknown coefficients. In general, the result is not unique, as stated above. The expression for $P_{\alpha\beta}$ used in our calculations is given explicitly in Appendix A.

On length scales large compared to the width of an interface, the interface can be viewed as a mathematical surface with surface tension σ and bending rigidity κ. In Appendix B, we show how the pressure tensor is related to the surface tension and the bending rigidity. Thereby we obtain the surface tension σ and the elastic modulus κ,

$$\sigma = \omega \int_{-\infty}^{\infty} \mathrm{d}z \left\{ 2g_\phi \bar{\phi}'^2 + 2g_\psi \bar{\psi}'^2 + 2l^2\gamma_2 \bar{\psi}\bar{\phi}'^2 + 4l^4\gamma_3 \bar{\psi}\bar{\phi}''^2 \right\}, \tag{11}$$

$$\kappa = \omega \int_{-\infty}^{\infty} \mathrm{d}z 2l^4\gamma_3 \bar{\psi}\bar{\phi}'^2, \tag{12}$$

for an almost flat interface with average normal in the z-direction, whose density profiles are $\bar{\phi}(z)$ and $\bar{\psi}(z)$; the prime denotes differentiation with respect to z. Here it is assumed that $\bar{\phi}$ and $\bar{\psi}$ are constant for $|z| \to \infty$.

From equations (11, 12) we can estimate how the length of the surfactants l affects the surface tension and bending rigidity purely from dimensional arguments. Assume l to be the only relevant length scale near the interface. Then its width is proportional to l, and $\bar{\phi}' \propto \bar{\phi}/l$. This leads to a reduction of the surface tension proportional to l due to the γ_2 term in equation (11) and a bending rigidity $\kappa \propto l^3$. The latter is the same dependence as described in reference [27] and agrees with the dependence of the bending rigidity of a thin plate on its thickness.

The knowledge of the interfacial properties in terms of σ and κ makes a quantitative comparison both with models formulated in terms of mathematical surfaces and with experiments possible. For the parameters chosen above, the tension and bending rigidity are found to be $\sigma/\omega = -0.0113$ and $\kappa/\omega = 0.119$ by minimization of equation (2); this leads to an initial instability as given by equation (1) for all wavelengths larger than 20 lattice units.

It has been shown in a reference [30] for an one-order-parameter free energy that the lattice Boltzmann approach indeed has the same large-scale dynamics as a mathematical surface controlled by σ and κ, with values calculated from expressions analogous to equations (11, 12).

3 The method

To solve the macrodynamics of the multi-phase flow given by equations (3–6), we use the lattice Boltzmann approach [23,22]. Within this method, the dynamics is not defined in terms of the hydrodynamic fields ρ, $\mathbf{v}$, ϕ and ψ, but in terms of velocity distributions $f_i(\mathbf{r},t)$, $g_i(\mathbf{r},t)$ and $h_i(\mathbf{r},t)$ for each of the densities ρ, ϕ and ψ. $f_i(\mathbf{r},t)$ is the probability density of the field ρ at position $\mathbf{r}$ and time t in the velocity state i with velocity $\mathbf{e}_i$. Analogous statements apply for $g_i(\mathbf{r},t)$ and $h_i(\mathbf{r},t)$. It is at the heart of the lattice Boltzmann method that only a minimum number of velocity states is taken into account. Here we work in two dimensions on a square lattice with $n = 9$ velocity states which are the zero velocity ($i = 0$), the nearest ($i = 1 \ldots 4$) and next-nearest neighbor ($i = 5 \ldots 8$) vectors on the square lattice. The dynamics of the lattice Boltzmann method is defined by

$$f_i(\mathbf{r} + \mathbf{e}_i, t+1) - f_i(\mathbf{r},t) = -\frac{1}{\tau}\left(f_i(\mathbf{r},t) - f_i^{\mathrm{eq}}(\mathbf{r},t)\right), \tag{13}$$

where f^{eq} is the equilibrium distribution and τ is a relaxation time [19,20]. Note that the timestep is equal to unity. This equation is basically the Boltzmann equation on a lattice for a finite set of velocity states with a BGK relaxation ansatz for the collision operator [33]. For $g_i(\mathbf{r},t)$ and $h_i(\mathbf{r},t)$ analogous equations apply; this introduces two more equilibrium distributions g_i^{eq} and h_i^{eq} with relaxation times τ_ϕ and τ_ψ, which are both taken to be $1/2 + \theta$ with $\theta = 1/(2\sqrt{3})$ (see below).

The "macrodynamic" quantities mass density ρ, momentum density $\rho\mathbf{v}$ and the densities ϕ and ψ are defined within the lattice Boltzmann approach as moments of the "microscopic" distributions,

$$\rho(\mathbf{r},t) = \sum_{i=0}^{n} f_i(\mathbf{r},t), \quad \rho(\mathbf{r},t)\mathbf{v}(\mathbf{r},t) = \sum_{i=0}^{n} f_i(\mathbf{r},t)\mathbf{e}_i \tag{14}$$

$$\phi(\mathbf{r},t) = \sum_{i=0}^{n} g_i(\mathbf{r},t), \quad \psi(\mathbf{r},t) = \sum_{i=0}^{n} h_i(\mathbf{r},t). \tag{15}$$

Conditions for the right hand side of equation (13) and thus for the equilibrium distributions arise from the requirement that these quantities have to be conserved by the dynamics of equation (13) and its corresponding equations for g_i and h_i. The equilibrium distributions f_i^{eq}, g_i^{eq} and h_i^{eq} themselves have to fulfill equations (14, 15) when they are inserted into them instead of f_i, g_i and h_i.

It has been shown in references [21,28] that both the macrodynamic equations, equations (3–6), and the thermodynamic behavior, as given by the free energy (2), are simulated, if — in addition to equations (14, 15) — the equilibrium distributions satisfy

$$\sum_{i=0}^{n} g_i^{\mathrm{eq}}\mathbf{e}_i = \phi\mathbf{v}, \quad \sum_{i=0}^{n} h_i^{\mathrm{eq}}\mathbf{e}_i = \psi\mathbf{v} \tag{16}$$

and

$$\begin{aligned}
\sum_{i=0}^{n} f_i^{\mathrm{eq}} e_{i\alpha}e_{i\beta} &= P_{\alpha\beta} + \rho v_\alpha v_\beta \\
\sum_{i=0}^{n} g_i^{\mathrm{eq}} e_{i\alpha}e_{i\beta} &= \tilde{\Gamma}_\phi \mu_\phi \delta_{\alpha\beta} + \phi v_\alpha v_\beta, \\
\sum_{i=0}^{n} h_i^{\mathrm{eq}} e_{i\alpha}e_{i\beta} &= \tilde{\Gamma}_\psi \mu_\psi \delta_{\alpha\beta} + \psi v_\alpha v_\beta.
\end{aligned} \tag{17}$$

The latter equations relate the equilibrium distributions to the thermodynamic equations of state, the pressure tensor $P_{\alpha\beta}$ and the chemical potentials μ_ϕ and μ_ψ. Explicit expressions for $f_i^{\rm eq}$, $g_i^{\rm eq}$ and $h_i^{\rm eq}$ are obtained by using an ansatz for the equilibrium distributions [28,21]. Details are given in Appendix C.

One time step of the emerging lattice Boltzmann algorithm consists of four consecutive steps. First, the macrodynamic quantities $\mathbf{v}$, ρ, ϕ and ψ are calculated from the actual distributions f_i, g_i and h_i by using equations (14, 15). Then the equations of state, equations (7, A.2) are evaluated. The third step is to determine the equilibrium distributions $f_i^{\rm eq}$, $g_i^{\rm eq}$ and $h_i^{\rm eq}$ according to equation (C.4). Finally, the distributions at time $t+1$ are calculated by means of the lattice Boltzmann timestep (13) for each distribution.

The choice $\tau_\phi = \tau_\psi = 1/2 + \theta$ with $\theta = 1/(2\sqrt{3})$ is crucial to approximate Galilean invariance as closely as possible on the lattice [21]. Thus we are left with three microdynamic parameters τ, $\tilde{\Gamma}_\phi$ and $\tilde{\Gamma}_\psi$ which determine the viscosity ν and the mobilities Γ_ϕ and Γ_ψ of the macrodynamic equations (3–6). The relations

$$\nu = \frac{1}{6}(2\tau - 1), \quad \Gamma_\phi = \theta\tilde{\Gamma}_\phi, \quad \Gamma_\psi = \theta\tilde{\Gamma}_\psi \qquad (18)$$

can be derived from a Chapman-Enskog expansion [34,21]. The mobilities Γ_ϕ and Γ_ψ are proportional to the diffusion constants of the densities ϕ and ψ as can be seen from equations (5, 6).

4 Simulations

The process of spontaneous emulsification is studied by preparing an initially planar oil-water interface parallel to the x-axis in a two-dimensional system. The direction normal to the interface is taken to be the z-direction. By a reduction of γ_2 this interface is quenched into the lamellar phase. However, the interface remains metastable due to the lack of any perturbations. To start the emulsification process we perturb the quenched but equilibrated planar field $\phi(z)$ by a tiny capillary wave with amplitude $\epsilon = 0.01$ and wave number k,

$$\phi(z) \to \phi(z + \epsilon\sin(kx)) \approx \phi(z) + \epsilon\sin(kx)\frac{\partial\phi(z)}{\partial z}\,. \qquad (19)$$

As ϵ can be regarded to be infinitesimal compared to the width of the interface of $\xi \approx 3$ and the lattice spacing of unity, there is no need to perturb ψ or v, too.

We choose periodic boundary conditions along the x-direction and impose forced boundary conditions [35,36] along the z-direction, with $v_z = 0$, $\phi = \pm\phi_{\rm e}$ and $\psi = 0.05$, in order to mimic an infinite bulk phase of either oil ($\phi = -\phi_{\rm e}$) or water ($\phi = +\phi_{\rm e}$). Here $\phi_{\rm e}$ is the equilibrium value of ϕ of the bulk oil and water phases for a given surfactant concentration ψ. These boundary conditions act like a reservoir for the surfactants, because an unlimited amount of surfactant may diffuse from the boundaries into the system.

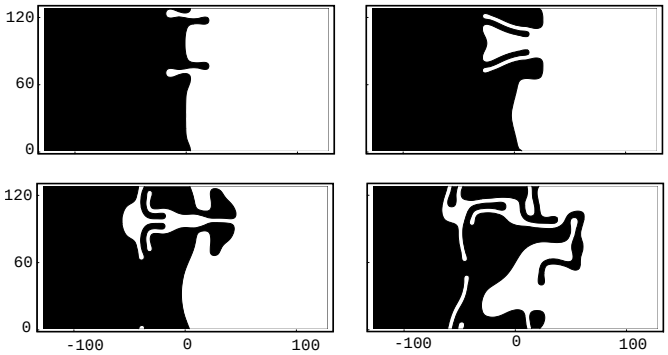

Fig. 1. Time series of the emulsification process for $\nu = 0.1$ and $\Gamma_\psi = 0.3\,\theta$ at times $t = 2 \times 10^5$, $t = 4 \times 10^5$, $t = 6 \times 10^5$ and $t = 10 \times 10^5$ from top left to bottom right. Regions with $\phi < 0$ are colored black, those with $\phi > 0$ white. The lattice size is $L_x = 128$ and $L_z = 256$.

We use square lattices with $L_x = 32$ or $L_x = 128$ lattice sites along the x-direction and $L_z = 256$ lattice sites along the z-direction. These sizes were chosen to allow for an instability according to equation (1) to develop and to reduce the influence of the boundaries perpendicular to the interface. Each run was performed over one million time steps.

In general, the dynamical behavior of a multicomponent fluid for fixed initial and boundary conditions is governed by its viscosity and diffusion constants. As we expect the diffusion of the surfactant and the convection to be important, we probe the system by varying the viscosity ν and the mobility Γ_ψ, but keep $\Gamma_\phi = 0.1\,\theta$ constant.

5 Results

5.1 Phenomenology

The morphology, which develops during the emulsification process, depends on the kinetic parameters Γ_ψ and ν. In turn, the dynamics itself is influenced by the morphology, since the forces, which the interface exerts on the fluid, depend on its area and curvature. We find two growth regimes, one for *fast diffusion* with $\Gamma_\psi > 0.1\,\theta$, and one for *slow diffusion* with $\Gamma_\psi < 0.1\,\theta$.

The positions of the oil-water interface for different times and $\Gamma_\psi = 0.3\,\theta$, $\nu = 0.1$ is shown in Figure 1. After a finger has formed perpendicular to the interface, the finger itself becomes unstable and a *secondary instability* develops. This behavior is to be expected, because any interface between bulk-regions of oil and water is unstable after the quench into the lamellar phase. This result resemble the experimental observation of finger-like structures, which occur during spontaneous emulsification [5]. We want to mention parenthetically that a completely different mechanism for spontaneous emulsification, where the oil penetrates into the surfactant bilayer of vesicles and lets them "explode", has also been observed [10].

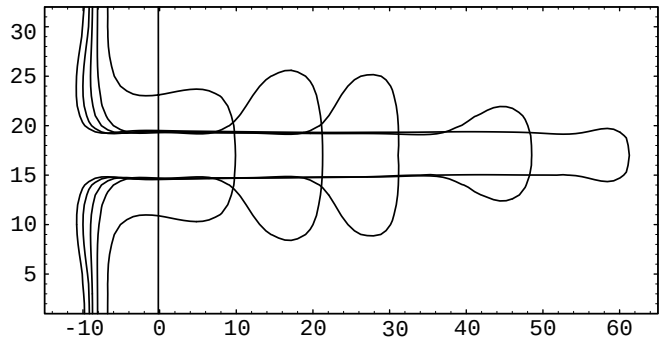

Fig. 2. Position of the interface at times $t = 0$, $t = 2 \times 10^5$, $t = 4 \times 10^5$, $t = 6 \times 10^5$, $t = 8 \times 10^5$ and $t = 1 \times 10^6$. The kinetic parameters are $\Gamma_\psi = 0.1\,\theta$ and $\nu = 0.1$. Note the different scales in the x and z directions. The lattice size is $L_x = 32$ and $L_z = 256$. Only a fraction of the system is displayed in the z direction.

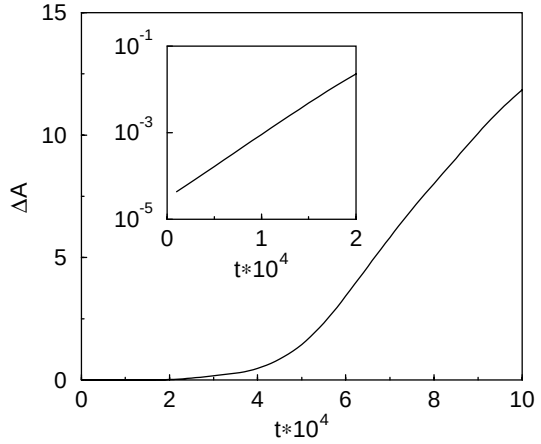

Fig. 3. Growth of the excess area ΔA *versus* time t for $\Gamma_\psi = 0.1\,\theta$ and $\nu = 0.1$. For $t > 5 \times 10^4$ there is a linear growth $\Delta A(t) \propto \beta t$. The inset shows a semi-logarithmic plot for the very early stages, $t < 2 \times 10^4$, where $\Delta A(t) \propto \exp(\alpha t)$.

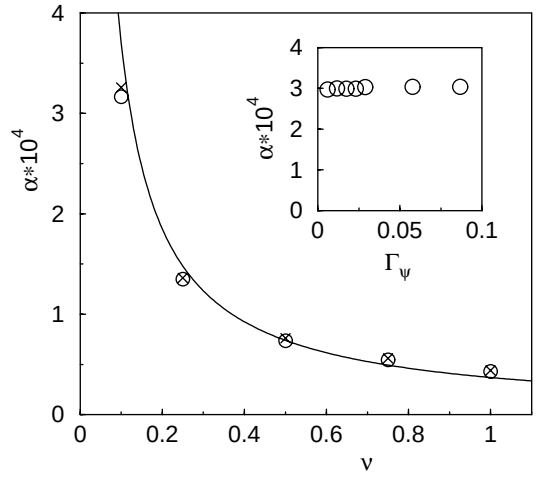

Fig. 4. Growth exponent α for the very early stages, $t < 2 \times 10^4$, as a function of the viscosity ν for $\Gamma_\psi = 0.02\,\theta$ ($\circ$) and $\Gamma_\psi = 0.2\,\theta$ ($\times$). The solid line shows a fit to a $\alpha = \alpha_0/\nu$ behavior with $\alpha_0 = 3.7 \times 10^{-5}$. The inset shows that α does not depend on Γ_ψ (with data for $\nu = 0.1$).

For low values of the mobility of ψ, *i.e.* $\Gamma_\psi < 0.1\,\theta$, and small systems ($L_x = 32$) always a *single* finger forms, which grows perpendicular to the initial interface, see Figure 2. There are no secondary instabilities, which lead to a growth in a different direction. We attribute this behavior to the fact that at low values of Γ_ψ not enough surfactant diffuses to the interface to build up a secondary instability. The morphology is thus dynamically stabilized. In addition, there is a stabilizing effect due to the attractive interactions between two interfaces [37].

Thus, there is in general a mutual dependence of dynamics and morphology which is difficult to disentangle. Therefore we consider here only the case $\Gamma_\psi < 0.1\,\theta$ for the late stages, where the morphology is approximately independent of time.

5.2 Initial dynamics

For the initial states, *i.e.* as long as no overhangs occur, the entire dynamics can be described by the position $h(x,t)$ of the interface which is known in differential geometry as the Monge representation of a surface. Here we focus on the excess area

$$\Delta A(t) = \int_0^{L_x} \mathrm{d}x \left(\sqrt{1 + (\nabla h(x,t))^2} - 1 \right) \qquad (20)$$

of the interface compared to the area of the planar interface. We can distinguish two different behaviors of $\Delta A(t)$ for very early and for somewhat later times after the excitation of a capillary wave. The early dynamics of $\Delta A(t)$ is found to be

$$\Delta A(t) \propto \mathrm{e}^{\alpha t}, \quad \text{with} \quad \alpha \propto \frac{1}{\nu} \qquad (21)$$

and α *independent* of Γ_ψ, see Figures 3 and 4. We find that the dependence of α on the wave number k, the surface tension σ and the bending rigidity κ agrees qualitatively with the prediction of equation (1), *i.e.* $\alpha \propto 2\lambda(k)$. However, $\alpha/(2\lambda(k))$ is roughly 2 instead of unity. At later times, there is a crossover to a linear growth of the excess area,

$$\Delta A(t) \propto \beta t, \quad \text{with} \quad \beta \propto (\Gamma_\psi)^b \quad \text{and} \quad b \approx \frac{1}{3}\,, \qquad (22)$$

compare Figure 5. Despite the fact that the data cover only about one order of magnitude, a value of $b \geq 1/2$ can certainly be ruled out. The dependence of β on the viscosity ν is the same as for α, *i.e.* $\beta \propto 1/\nu$. The linear growth behavior, equation (22), ends due to the breakdown of the Monge representation. These observations support the idea of a *hydrodynamic instability*, as it is reflected by the exponential growth, with a growth constant inversely proportional to the viscosity ν, and a crossover to a *diffusion controlled* behavior, which is linear in time.

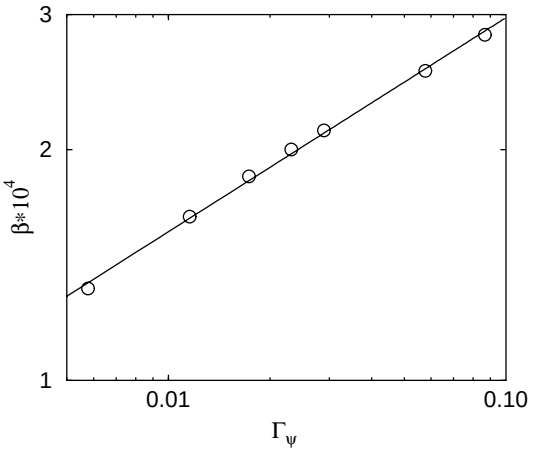

Fig. 5. Linear growth rate β *versus* the mobility Γ_ψ for $\nu = 0.1$ in a double-logarithmic plot. The solid line is a fit to the power law $\beta = \beta_0(\Gamma_\psi)^b$, which gives $b = 0.28 \pm 0.01$ and $\beta_0 = 5.65 \times 10^{-4}$.

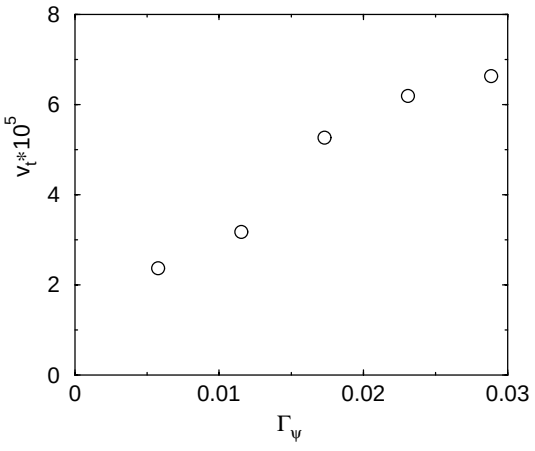

Fig. 6. Velocity of the tip v_t as a function of the mobility Γ_ψ for $\nu = 0.1$. Only those values of Γ_ψ are plotted, for which the tip advances perpendicular to the initial interface.

Remarkably, we find that $\Delta A \propto \Gamma_\psi^{1/3} t$, whereas one would expect naively the growth of the interface, $\mathrm{d}(\Delta A)/\mathrm{d}t$, to be proportional to the flux $\Gamma_\psi \nabla\psi$ of surfactants diffusing towards the interface, and thus $\Delta A \propto \Gamma_\psi^{1/2} t^{1/2}$ (since the concentration varies on the length scale of the diffusion length $l_d \propto (\Gamma_\psi t)^{1/2}$).

Due to different choices of initial conditions, our results for the initial dynamics cannot be compared directly with the theory of Granek, Ball and Cates [12]. For a situation, where the amphiliphile has to *diffuse* towards the interface to make σ negative, Granek *et al.* predict an initial growth law $\Delta A_{\mathrm{th}}(t) \propto \Gamma_\psi^{5/4} t^{3/4} \exp(a t^{5/2} \Gamma_\psi^{3/2}/\nu)$, followed by a crossover to a linear, diffusion-controlled growth. While the first, exponential stage of the growth process certainly depends strongly on the initial conditions, the second stage of diffusion-controlled, linear growth seems to be more universal.

5.3 Late dynamics

At late times, $h(x)$ is no longer defined. The dynamics can then be characterized by the velocity v_t of the "finger" which advances into the bulk phase. For the remainder of this paper we restrict our attention to values of Γ_ψ, for which the instability grows perpendicular to the interface. Thus the overall shape of the instability can be regarded to be independent on Γ_ψ and ν. In particular, the finger has always the same thickness, which can be identified as the distance between neighboring interfaces in the lamellar phase. This reflects the fact that we study the dynamics of the phase transition from oil-water coexistence into the lamellar phase.

After the initial phase the tip advances with *constant* velocity v_t, thus its position $Z(t)$ can be fitted accurately to a $Z(t) = v_t t + Z_0$ law, from which v_t is determined. The existence of a stage with constant velocity v_t of the tip indicates that there is a balance between the growth of the interface and the driving capillary force. As the growth of the interface is an amphiphile-consuming process, whereas a constant driving force requires a constant concentration of amphiphiles at the interface, there must be a constant total flux of amphiphiles to the interface.

This flux can either be due to convection or diffusion. A visual analysis of typical flow patterns shows that convection is mainly *parallel* to the interface. Thus diffusion is the main transport mechanism of amphiphiles to be considered. The situation is similar to dendritic growth phenomena [38], where a dendrite growths with constant velocity into the undercooled melt. For dendritic growth the velocity is governed by the diffusion of the latent heat, which is produced during solidification and has to be transported away from the solid-melt interface in order for solidification to proceed. The temperature field of dendritic growth, which corresponds to the density ψ of the amphiphiles, has its largest gradients near the tip of the dendrite and thus the heat flux is mainly located in the vicinity of the tip.

Support for this picture is provided by Figure 8, where we show the spatial distribution of the absolute value of the diffusional flux

$$j_\psi^{\mathrm{d}}(x,z) = \Gamma_\psi |\nabla \mu_\psi(x,z)| \tag{23}$$

of the amphiphiles. This figure shows that, indeed, diffusion takes place mainly at the front end of the tip and near the rear interface. In between the tip and the rear interface, there is almost no diffusion, because there the amphiphile is already depleted.

As can be expected from this discussion, the tip velocity v_t increases as a function of Γ_ψ; unfortunately, the scatter of the data shown in Figure 6 is too large to allow for a more quantitative analysis. We can attribute the noise in the data to the fact that the shape of the tip is sensitive to the value of Γ_ψ. We conclude from these results that the *diffusion* of the surfactant controls the velocity of the emulsification process also in its late stages.

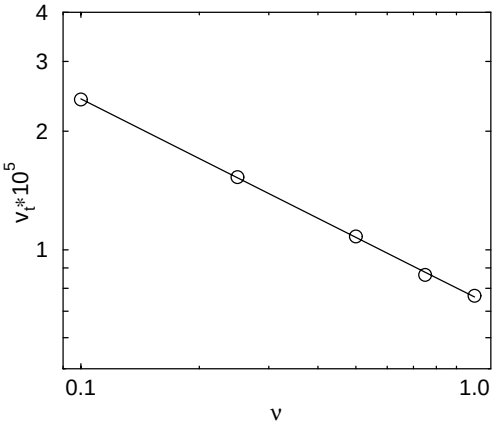

Fig. 7. Tip velocity v_t as a function of the viscosity ν. The value of the mobility is $\Gamma_\psi = 0.02\,\theta$. Note that both axes are logarithmic. The solid line is a fit to a power law, which yields $v_t \propto \nu^{-1/2}$.

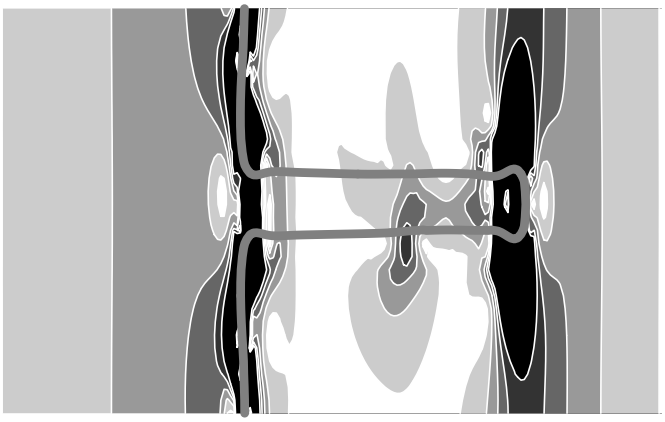

Fig. 8. Spatial distribution of the absolute value of the diffusional flux of the amphiphiles. This snapshot was taken from the same run for which the interface is displayed in Figure 2 and corresponds to the latest time shown there. Dark colors correspond to a high flux, the position of the interface is indicated by the bold grey line.

However, there is a crucial difference between spontaneous emulsification and dendritic growth. The finger in the former case is fluid itself, so that convective effects lead to a dependence of v_t on the viscosity ν, which is found to exhibit a

$$v_t \propto \nu^{-0.501\pm0.005} \tag{24}$$

behavior, see Figure 7. This dependence is much weaker than what would be expected from a simple Stokes flow with a constant driving force f, for which the velocity field is given by

$$v_\alpha(\mathbf{r}) = \int \mathrm{d}\mathbf{r}'\, O_{\alpha\beta}(\mathbf{r}-\mathbf{r}') f_\beta(\mathbf{r}') \tag{25}$$

where

$$O_{\alpha\beta}(\mathbf{r}) = \frac{1}{8\pi\rho\nu|\mathbf{r}|}\left(\delta_{\alpha\beta} + \frac{r_\alpha r_\beta}{|\mathbf{r}|^2}\right) \tag{26}$$

is the Oseen tensor in three dimensions. The Oseen tensor in two dimensions is more complicated, but shows the same ν^{-1} dependence on the viscosity. Therefore all velocities, including v_t, would scale as ν^{-1}.

In order to obtain some insight into the transport mechanisms, we study the total diffusional and convective fluxes of ϕ and ψ,

$$J_\phi^{\mathrm{c}} = \int \mathrm{d}x\mathrm{d}z|\phi(x,z)\mathbf{v}(x,z)|,\ J_\psi^{\mathrm{c}} = \int \mathrm{d}x\mathrm{d}z|\psi(x,z)\mathbf{v}(x,z)|, \tag{27}$$

$$J_\phi^{\mathrm{d}} = \Gamma_\phi \int \mathrm{d}x\mathrm{d}z|\nabla\mu_\phi(x,z)|,\ J_\psi^{\mathrm{d}} = \Gamma_\psi \int \mathrm{d}x\mathrm{d}z|\nabla\mu_\psi(x,z)|. \tag{28}$$

The total fluxes displayed in Figure 9 where obtained by averaging over all timesteps, except the initial stage (the first 2×10^5 timesteps).

The diffusional and convective fluxes for both ϕ and ψ increase in a similar manner with Γ_ψ, which reflects the fact that the diffusion of the amphiphiles controls the dynamics. The convective fluxes as a function of ν obey the power laws

$$J_\phi^{\mathrm{c}} \propto \nu^{-0.72\pm0.02} \quad \text{and} \quad J_\psi^{\mathrm{c}} \propto \nu^{-0.54\pm0.02} \tag{29}$$

which again leads to a weaker dependence on ν than for a Stokes-flow. More surprisingly, the diffusional fluxes J_ϕ^{d} and J_ψ^{d} depend on the viscosity with approximately the same power laws. This implies that they are coupled to the convective motion of their densities. We can only speculate about the origin of this behavior. One possible explanation is that the convection transports amphiphiles towards the rear interface, thus increasing the density of the amphiphiles in a region where diffusion acts. A second reason might be that the tip advances faster with decreasing viscosity ν into amphiphile-rich regions, causing a steeper gradient of the chemical potential. The same reasoning holds for the fluxes of the oil-water density difference ϕ.

The magnitude of the fluxes shows that oil and water are mainly transported by convection. The Peclet number for ϕ, which is defined by the ratio of the convective and the diffusive flux, takes values between 10 and 15. The Peclet number for the amphiphiles is lower by a factor 2 to 3; this indicates that diffusion is more important for the amphiphile than for oil and water.

6 Summary and discussion

In this paper we have used a lattice Boltzmann approach combined with a Ginzburg-Landau free energy to study the process of spontaneous emulsification. We find the mixing of oil and water to be dominated by convection. However, the speed of the emulsification process is controlled in the first place by the diffusion of the amphiphiles

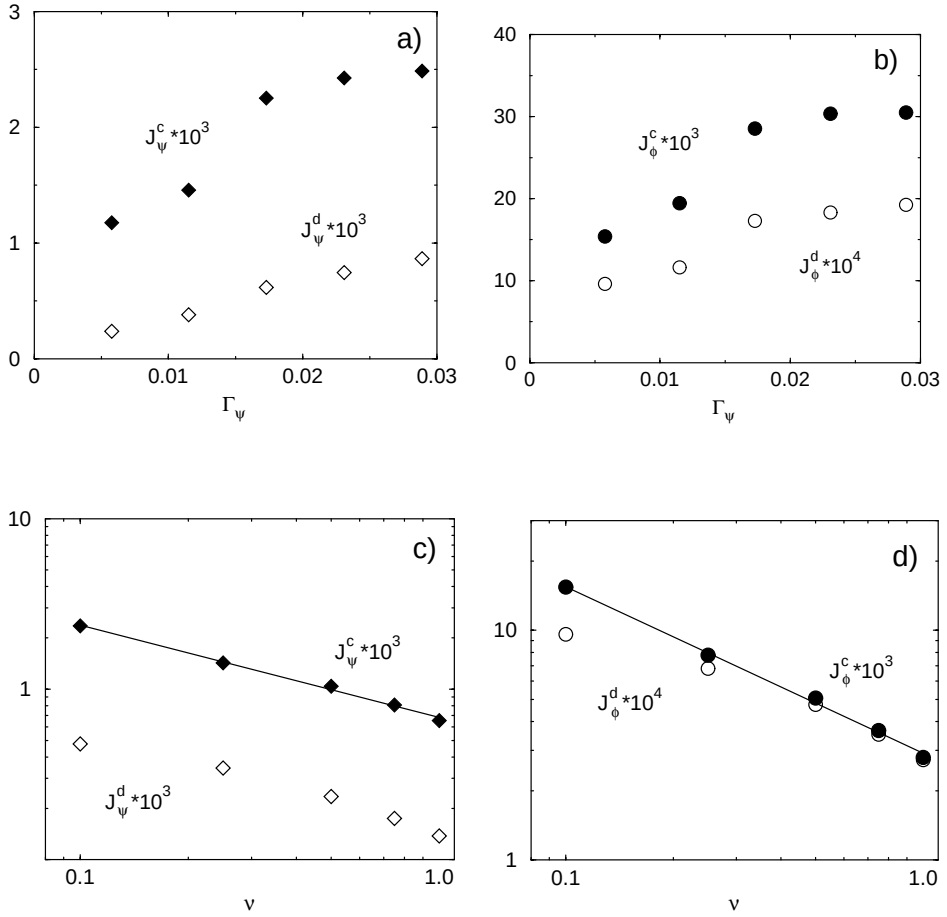

Fig. 9. Time and volume averages of the fluxes as a function of Γ_ψ and ν. Open symbols correspond to the diffusive fluxes, closed symbols to convective fluxes. Note that, in (b) and (d), the diffusive fluxes of ϕ, J^{d}_ϕ, are scaled by an extra factor of 10. The viscosity in (a) and (b) is $\nu = 0.1$, the mobility in (c) and (d) $\Gamma_\psi = 0.02\theta$.

and thus by Γ_ψ. The influence of the viscosity is less pronounced as in a simple Stokes flow.

We interpret this behavior as a non-trivial coupling of convection and diffusion, which can be split into three parts. First, the diffusion of the surfactants to the interface controls the surface tension and thus the driving force of the emulsification process. Second, this driving force is balanced by the viscous stresses in the fluid and causes a convective transport of oil and water. This transport thus increases with Γ_ψ and, due to the convective part, decreases with ν. The ν dependence is weakened by the diffusional contributions. Third, there is a feedback of the convection to the diffusional transport, which makes the diffusional flux depend on the viscosity ν. Thus, to describe the emulsification process correctly, it is crucial to use a three component model, in which the amphiphile density is explicitly taken into account.

We restricted ourselves to two dimensions in order to minimize the computational effort. Usually, the dimensionality is crucial for multi-phase flows due to the presence of the Rayleigh instability [14] in $d = 3$ and its absence in $d = 2$. However, in surfactant systems the surface tension, which is the driving force of the Rayleigh instability, is very low or even zero. In addition, surfactants can stabilize cylindrical arrangements of oil in water and *vice versa* as indicated by the existence of a hexagonal phase. Therefore we believe our two-dimensional simulations to be comparable with experiments, even though the values of the growth rates and exponents may be different in three dimensions. Indeed, cylindrical arrangements of oil in water which don't show a Rayleigh instability have been observed in spontaneous emulsification [5].

Compared to dendritic growth phenomena, spontaneous emulsification is similar in the respect that diffusion of a field (amphiphile density and temperature, respectively) leads to the formation of a tip perpendicular to the initial interface, because growth is faster in regions with larger field gradients. However, there are several differences between dendritic growth and spontaneous emulsification, which prohibit a closer analogy. For dendritic growth, convection is irrelevant, the driving force is due to a phase transition in the bulk and the positive surface tension has a stabilizing effect. In contrast, spontaneous emulsification is driven by a negative surface tension, bending rigidity smoothens the interface at short length scales, and convection strongly affects the growth velocity.

Appendix A: Pressure tensor

The ideal (thermodynamic) part p_0 of the pressure tensor is obtained from equation (8),

$$\begin{aligned} p_0 = \omega\{&T\rho + 3\phi^4 - 2\phi_b^2\phi^2 + 2s\psi^2 - 2g_\phi\phi\nabla^2\phi \\ &- g_\phi(\nabla\phi)^2 - 2g_\psi\psi\nabla^2\psi - g_\psi(\nabla\psi)^2 \\ &+ 2\gamma_1\psi\phi^2 - 2\gamma_2\phi(\nabla\psi)(\nabla\phi) - 2\gamma_2\psi\phi\nabla^2\phi \\ &+ 2\gamma_3\psi\phi\nabla^2\nabla^2\phi + 4\gamma_3\phi(\nabla\psi)(\nabla\nabla^2\phi) \\ &+ 2\gamma_3\phi(\nabla^2\psi)(\nabla^2\phi)\} \end{aligned} \tag{A.1}$$

where irrelevant constant terms have been neglected. As there is no formula available for the non-ideal part of the pressure tensor $\tilde{P}_{\alpha\beta}$, we proceed by an ansatz constructed in the following way. For dimensional reasons, equations (2, 9) imply that all terms of the pressure tensor proportional to, say, γ_2 must be proportional to $\psi\phi^2$ and of second order in the spatial derivatives. The ansatz for the γ_2 contributions to $\tilde{P}_{\alpha\beta}$ therefore contains all possible combinations which meet these requirements, each with an undetermined coefficient. Using equation (9), we get a system of equations which relates these coefficients. Any solution of this system of equations gives a correct expression for $\tilde{P}_{\alpha\beta}$. Each two solution differ by a physically irrelevant tensor $\Lambda_{\alpha\beta}$, whose divergence is zero. The expression for the non-ideal part of the pressure tensor used in this paper is

$$\begin{aligned} \tilde{P}_{\alpha\beta} = \omega\{&2g_\phi(\partial_\alpha\phi)(\partial_\beta\phi) + 2g_\psi(\partial_\alpha\psi)(\partial_\beta\psi) \\ &+ 2\gamma_2\psi(\partial_\alpha\phi)(\partial_\beta\phi) \\ &- 2\gamma_3[(\partial_\alpha\psi)(\partial_\beta\phi)(\nabla^2\phi) + (\partial_\beta\psi)(\partial_\alpha\phi)(\nabla^2\phi)] \\ &- 2\gamma_3[\psi(\partial_\alpha\phi)(\partial_\beta\nabla^2\phi) + \psi(\partial_\beta\phi)(\partial_\alpha\nabla^2\phi)] \\ &+ 2\gamma_3[\psi(\nabla^2\phi)^2 + (\nabla\psi)\cdot(\nabla\phi)(\nabla^2\phi) \\ &+ \psi(\nabla\phi)\cdot(\nabla\nabla^2\phi)]\delta_{\alpha\beta}\}. \end{aligned} \tag{A.2}$$

Appendix B: Surface tension and bending rigidity

The connection between $P_{\alpha\beta}$ and σ is well established [39],

$$\sigma = \int \mathrm{d}z\ (P_\mathrm{N}(z) - P_\mathrm{T}(z)), \tag{B.1}$$

where P_N is the normal and P_T the tangential component of the pressure tensor. For an interface with normal in the z-direction, $P_\mathrm{N}(z) = P_{zz}(z)$ and $P_\mathrm{T}(z) = P_{xx}(z)$.

The bending rigidity κ has not been determined from $P_{\alpha\beta}$ so far. Here we show how such an expression can be derived. Consider an almost flat interface $h(x,y)$ with its normal in the z-direction. The free energy of this interface is given by the curvature Hamiltonian, which reads

$$\mathcal{H}[h] = \int \mathrm{d}x\mathrm{d}y \left\{\frac{\sigma}{2}(\nabla_\parallel h)^2 + \frac{\kappa}{2}(\nabla_\parallel^2 h)^2\right\} \tag{B.2}$$

to lowest order in $h(x,y)$ [40,41]. Here $\nabla_\parallel$ refers to the nabla operator in the xy plane. The normal component of the force, which this interface exerts on the fluid, is

$$F_z = -\frac{\delta\mathcal{H}}{\delta h} = \left\{\sigma\nabla_\parallel^2 - \kappa(\nabla_\parallel^2)^2\right\} h(x,y). \tag{B.3}$$

On the other hand, this force can be calculated directly from the pressure tensor. The force in z-direction at a given position in the fluid is $\partial_\beta P_{z\beta}$, which can be obtained from equation (9); the superposition principle then leads to the force

$$F_z = \int_{-\infty}^{\infty} \mathrm{d}z \partial_\beta P_{z\beta}, \tag{B.4}$$

which the whole interface exerts on the fluid. The two forces (B.3, B.4) for the same height function $h(x,y)$ of the interface must be identical. To express equation (B.4) in terms of $h(x,y)$, ϕ and ψ are expanded for an almost planar interface about the equilibrium density profile $\bar{\phi}(z)$ and $\bar{\psi}(z)$ of a flat interface,

$$\phi(x,y,z) \approx \bar{\phi}(z + h(x,y)) \approx \bar{\phi}(z) + \bar{\phi}'(z)h(x,y) \tag{B.5}$$

$$\psi(x,y,z) \approx \bar{\psi}(z + h(x,y)) \approx \bar{\psi}(z) + \bar{\psi}'(z)h(x,y) \tag{B.6}$$

to lowest order in h, where $\phi' = \partial\phi/\partial z$ and $\psi' = \partial\psi/\partial z$. Equations (B.5, B.6) are inserted into equation (B.4). A comparison of equations (B.3, B.4) then yields σ and κ as given in equations (11, 12).

This derivation is not the only possible way to determine σ and κ for a Ginzburg-Landau-type theory. Previous calculations based on the comparison of the total Ginzburg-Landau free energy of spheres and cylinders with the curvature energy [37,42] or on a calculation of the free energy of capillary waves for both the Ginzburg-Landau model and the curvature Hamiltonian [43]. Of course, all three approaches are equivalent.

Appendix C: Equilibrium distributions

Each of the equilibrium distributions f_i^eq, g_i^eq and h_i^eq must fulfill equations of the form

$$\sum_{i=0}^{n} w_i^\mathrm{eq} = \chi, \quad \sum_{i=0}^{n} w_i^\mathrm{eq}\mathbf{e}_i = \chi\mathbf{v} \tag{C.1}$$

$$\sum_{i=0}^{n} w_i^\mathrm{eq} e_{i\alpha}e_{i\beta} = T_{\alpha\beta} + \chi v_\alpha v_\beta \tag{C.2}$$

where χ is either ρ, ϕ or ψ, and $T_{\alpha\beta}$ either $P_{\alpha\beta}$, $\tilde{\Gamma}_\phi\mu_\phi\delta_{\alpha\beta}$ or $\tilde{\Gamma}_\psi\mu_\psi\delta_{\alpha\beta}$, respectively. The ansatz used for w_i^eq on a two-dimensional square lattice is [20,21]

$$\begin{aligned} w_0^\mathrm{eq} &= A^{(0)} + C^{(0)}\mathbf{v}^2 \\ w_i^\mathrm{eq} &= A_{\alpha\beta}^{(1)} e_{i\alpha}e_{i\beta} + B^{(1)}\mathbf{e}_i\mathbf{v} + C^{(1)}\mathbf{v}^2 \\ &\quad + D^{(1)}(\mathbf{e}_i\mathbf{v})^2 \quad \text{for} \quad i = 1\ldots4 \\ w_i^\mathrm{eq} &= \frac{1}{4}\Big(A_{\alpha\beta}^{(1)} e_{i\alpha}e_{i\beta} + B^{(1)}\mathbf{e}_i\mathbf{v} \\ &\quad + C^{(1)}\mathbf{v}^2 + D^{(1)}(\mathbf{e}_i\mathbf{v})^2\Big) \quad \text{for} \quad i = 5\ldots8, \end{aligned} \tag{C.3}$$

which should be viewed as an expansion of $w_i^{\rm eq}$ for small velocities, which is rotational invariant in the velocity-dependent terms, and which allows for an possible anisotropy $A^{(1)}_{\alpha\beta}$ due to a non-isotropic pressure $P_{\alpha\beta}$. Higher orders in $\mathbf{v}$ or in the anisotropy can be neglected, because no conditions have to be fulfilled which would require their presence.

Determining the unknown coefficients of the ansatz from conditions (C.1) and (C.2), we obtain

$$\begin{aligned} w_0^{\rm eq} &= \chi - \frac{3}{4}(T_{xx}+T_{yy}) - \frac{2}{3}\chi\mathbf{v}^2 \\ w_i^{\rm eq} &= A^{(1)}_{\alpha\beta}e_{i\alpha}e_{i\beta} + \frac{1}{3}\chi\mathbf{e}_i\mathbf{v} - \frac{1}{6}\chi\mathbf{v}^2 + \frac{1}{2}\chi(\mathbf{e}_i\mathbf{v})^2 \\ &\quad \text{for} \quad i = 1\ldots 4 \\ w_i^{\rm eq} &= \frac{1}{4}A^{(1)}_{\alpha\beta}e_{i\alpha}e_{i\beta} + \frac{1}{12}\chi\mathbf{e}_i\mathbf{v} - \frac{1}{24}\chi\mathbf{v}^2 + \frac{1}{8}\chi(\mathbf{e}_i\mathbf{v})^2 \\ &\quad \text{for} \quad i = 5\ldots 8 \end{aligned} \tag{C.4}$$

where

$$A^{(1)}_{xx} = \frac{1}{8}(3T_{xx} - T_{yy}) = -A^{(1)}_{yy} \text{ and } A^{(1)}_{xy} = A^{(1)}_{yx} = \frac{1}{2}T_{xy}.$$

References

1. *Micelles, Membranes, Microemulsions and Monolayers*, edited by W.M. Gelbart, A. Ben-Shaul, D. Roux (Springer, Berlin, 1994).
2. G. Gompper, M. Schick, in *Self-Assembling Amphiphilic Systems*, Vol. 16 of *Phase Transitions and Critical Phenomena*, edited by C. Domb, J. Lebowitz (Academic Press, London, 1994).
3. W.J. Benton, K.H. Raney, C.A. Miller, J. Colloid Interface Sci. **110**, 363 (1986).
4. K.H. Raney, W.J. Benton, C.A. Miller, J. Colloid Interface Sci. **117**, 282 (1987).
5. J.C. Lim, C.A. Miller, Langmuir **7**, 2021 (1991).
6. J.C. Lim, C.A. Miller, C. Yang, Colloids Surf. **66**, 45 (1992).
7. C.A. Miller, K.H. Raney, Colloids Surf. A **74**, 169 (1993).
8. M.J. Rang *et al.*, J. Colloid Interface Sci. **175**, 440 (1995).
9. C.A. Miller, Tenside Surf. Det. **33**, 191 (1996).
10. N. Shahidzadeh, D. Bonn, J. Meunier, Europhys. Lett. **40**, 459 (1997).
11. *Dynamics and Instability of Fluid Interfaces*, *Lecture Notes in Physics*, edited by T.S. Sorensen (Springer, Berlin, 1979).
12. R. Granek, R.C. Ball, M.E. Cates, J. Phys. II France **3**, 829 (1993).
13. F. Brochard, J.F. Lennon, J. Phys. France **36**, 1035 (1975).
14. S. Chandrasekhar, *Hydrodynamic and Hydromagnetic Stability* (Dover, New York, 1961).
15. J. Burton, R. Prim, W. Slichter, J. Chem. Phys **21**, 1987 (1953).
16. G.R. McNamara, G. Zanetti, Phys. Rev. Lett. **61**, 2332 (1988).
17. F.J. Higuera, S. Succi, R. Benzi, Europhys. Lett. **9**, 345 (1989).
18. F.J. Higuera, S. Succi, Europhys. Lett. **8**, 517 (1989).
19. H. Chen, S. Chen, W.H. Matthaeus, Phys. Rev. A **45**, 5339 (1992).
20. Y.H. Qian, D. d'Humières, P. Lallemand, Europhys. Lett. **17**, 479 (1992).
21. M.R. Swift, E. Orlandini, W.R. Osborn, J.M. Yeomans, Phys. Rev. E **54**, 5041 (1996).
22. D.H. Rothmann, S. Zaleski, *Lattice-gas cellular automata* (Cambridge Univ. Press, Cambridge, 1997).
23. S. Chen, G.D. Doolen, Annu. Rev. Fluid Mech. **30**, 329 (1998).
24. D. Roux *et al.*, Europhys. Lett. **11**, 229 (1990).
25. D. Roux, C. Coulon, M.E. Cates, J. Phys. Chem. **96**, 4174 (1992).
26. G. Gompper, M. Schick, Phys. Rev. E **49**, 1478 (1994).
27. H. Woo, C. Carraro, D. Chandler, Phys. Rev. E **52**, 6497 (1995).
28. E. Orlandini, M.R. Swift, J.M. Yeomans, Europhys. Lett. **32**, 463 (1995).
29. G. Gonnella, E. Orlandini, J.M. Yeomans, Phys. Rev. Lett. **78**, 1695 (1997).
30. O. Theissen, G. Gompper, D.M. Kroll, Europhys. Lett. **42**, 419 (1998).
31. G. Gonnella, E. Orlandini, J.M. Yeomans, Phys. Rev. E **58**, 480 (1998).
32. R. Evans, Adv. Phys. **28**, 143 (1979).
33. P.L. Bhatnagar, E.P. Gross, M. Krook, Phys. Rev. **94**, 511 (1954).
34. S. Chapman, T. Cowling, *The Mathematical Theory of Non-uniform Gases* (Cambridge University Press, Cambridge, 1970).
35. D.R. Noble, S. Chen, J.G. Georgiadis, R.O. Buckius, Phys. Fluids **7**, 203 (1995).
36. Z. Lin, H. Fang, R. Tao, Phys. Rev. E **54**, 6323 (1996).
37. G. Gompper, S. Zschocke, Phys. Rev. A **46**, 4836 (1992).
38. J.S. Langer, Rev. Mod. Phys. **52**, 1 (1980).
39. J.S. Rawlinson, B. Widom, *Molecular Theory of Capillarity* (Clarendon Press, Oxford, 1982).
40. E. Helfrich, Z. Naturforsch. **28c**, 693 (1973).
41. P.M. Chaikin, T. Lubensky, *Principles of Condensed Matter Physics* (Cambridge University Press, Cambridge, 1995).
42. E.M. Blokhuis, Ber. Bunsenges. Phys. Chem. **100**, 313 (1996).
43. G. Gompper, M. Kraus, Phys. Rev. E **47**, 4289 (1993).